
Proceedings Paper:
Mullis, AM, Bollada, PC and Jimack, PK (2018) Phase-Field Modelling of Intermetallic Solidification. In: TMS 2018 147th Annual Meeting & Exhibition Supplemental Proceedings. TMS Annual Meeting & Exhibition 2018, 11-15 Mar 2018, Phoenix, USA. Springer, Cham , pp. 587-596. ISBN 978-3-319-72525-3

https://doi.org/10.1007/978-3-319-72526-0_55

Phase-field Modelling of Intermetallic Solidification

Andrew M Mullis[1a], *Peter C Bollada*[1] *and Peter K Jimack*[2]
[1]School of Chemical & Process Engineering,
[2]School of Computing,
University of Leeds, Leeds, LS2 9JT, UK.
[a]Corresponding Author: A.M.Mullis@leeds.ac.uk

Abstract

Many important intermetallic compounds display a faceted morphology during solidification close to equilibrium but adopt a more continuous, dendritic like morphology with increasing departure from equilibrium. We present a phase-field model of solidification that is able to both reproduce the Wulff shape at low driving force and to simulate a continuous transition from faceted to dendritic growth as the driving force is increased. A scaled ratio of the $(\text{perimeter})^2$ to the area is used to quantify the extent of departure from the equilibrium shape.

Key Words: Phase-field modelling, Faceted crystals, Intermetallics

Introduction

Phase-field modelling is widely used to simulate continuous (non-faceted) crystal morphologies, such as dendrites, during growth from the melt. Much less attention has been paid to the growth of faceted crystals as the phase-field rationale of approximating the sharp solid-liquid interface with one that is diffuse does not immediately lend itself to the solidification of such faceted crystals. Despite this, a number of methodologies for simulating faceted morphologies have been proposed [e.g. 1, 2, 3, 4, 5, 6].

Much of the interest in simulating faceted crystal growth has been stimulated by the study of Si and Ge due to their importance in the electronics industry. However, the growth of faceted crystals is also important within the light metals industry with regard to structural components. This is not only because Si is used extensively in Al casting alloys, producing a faceted/non-faceted eutectic but also because many of the most deleterious intermetallics formed due to impurity elements within Al-alloys are strongly faceted (e.g. θ-$Al_{13}Fe_4$ [7]).

It is well established that crystals that grow with faceted morphologies close to equilibrium progressively take on more continuous interface shapes with increasing departures from equilibrium, eventually adopting fully dendritic morphologies. This has been shown for the growth of pure semiconductors [8, 9], the Si phase in Al-Si eutectics [10] and for intermetallic phases [11]. Simulation of this particular aspect of faceted growth has however received very little attention.

Within phase-field the strong anisotropy required to produce faceted growth can be incorporated into the interfacial surface energy [1, 2, 3], the kinetic mobility [4, 5] or both [6]. Recent work has tended to favour the kinetic approach, but when considering the faceted to non-faceted transition mediated by high growth velocity this approach is problematic as the tendency towards faceting becomes stronger, rather than weaker, with increasing growth

velocity. There is a further problem in that, in the limit of vanishing growth velocity the kinetic anisotropy vanishes, giving rise to isotropic growth. In contrast, faceting introduced via the surface energy has the desirable properties that the faceted morphology is most pronounced at equilibrium and is progressively lost with increasing growth velocity. As such, this approach is a computationally expedient means of studying the faceted to non-faceted growth transition.

In this paper we use a phase-field model of faceted crystal growth mediated by a strong anisotropy in the interfacial surface energy in order to study the transition from faceted to dendritic growth with increasing growth velocity. As far as we are aware, the only previous work to simulate this type of transition using phase-field is [3], and then in the case of thermal growth only.

Phase-field Model

The equations for the evolution of the phase- (ϕ) and solute- (c) fields are given by:

$$\dot{\phi} = -M \frac{\delta F}{\delta \phi} \tag{1}$$

$$\dot{c} = \nabla \cdot D \nabla \frac{\delta F}{\delta c} \tag{2}$$

where D and M are the solute diffusivity and kinetic mobility respectively. F is the total free energy for the system, given by:

$$F = \int_{\Omega} G \, d^3x \tag{3}$$

with G being the free energy density given by:

$$G = g(\phi) G_{liq}(c,T) + \left(1 - g(\phi)\right) G_{sol}(c,T) + \omega \left[A(\nabla \phi) + 8\phi^2 \left(1 - \phi\right)^2 \right] \tag{4}$$

Here, $g(\phi) = \phi^2(3 - 2\phi)$ is a polynomial that interpolates between the bulk free energies for the liquid (G_{liq}) and solid (G_{sol}) phase respectively at concentration c and temperature T, ω is a scalar that governs the barrier height associated with the double well potential $8\phi^2(1 - \phi)^2$ and A is a function that governs the anisotropy. The most common model for weakly anisotropic materials displaying four-fold symmetry is:

$$A(\nabla \phi) = \tfrac{1}{2} \delta^2 \gamma(\nabla \phi) \cdot \gamma(\nabla \phi) \quad , \quad \text{with} \quad \gamma(\nabla \phi) = \left[1 + \varepsilon \cos 4\theta \right] \nabla \phi \tag{5}$$

where δ is a measure of the width of the diffuse interface and ε controls the strength of the anisotropy. θ is the angle of the outward pointing normal to the solid-liquid interface, given by:

$$\hat{\mathbf{n}} \equiv \frac{\nabla\phi}{|\nabla\phi|} = \begin{bmatrix} \cos\theta \\ \sin\theta \end{bmatrix} \tag{6}$$

In the simulations reported here we consider the growth of Si crystals from hypereutectic Al-Si at $c = 0.6$ (60 at.% Si). The bulk free energies for the solid and liquid phases are given by:

$$G_j(c,T) = cG_j^{Al}(T) + (1-c)G_j^{Si}(T) + \frac{RT}{v_m}\left[c\ln c + (1-c)\ln(1-c)\right] + G_j^{xs}(c,T) \tag{7}$$

Here j labels the phase (either liquid or solid), R is the gas constant and v_m the molar volume. G^i (i = Al, Si) are the free energy of the pure elements while G^{xs} is the excess free energy on mixing, which are given respectively by:

$$G_j^i = a_j^i + b_j^i T + c_j^i T\ln T + d_j^i T^2 + e_j^i T^3 + f_j^i T^{-1} + g_j^i T^7 + h_j^i T^{-9} \tag{8}$$

$$G_j^{xs}(c) = c(1-c)\sum_{m=0}^{4}\left(p_j^{(m)} + q_j^{(m)}T\right)(1-2c)^m \tag{9}$$

Equations (7)-(9) are the standard way of representing the thermodynamics of solution phases in CALPHAD. The coefficients *a-h* and *p-q* are obtained from version 5.0 of the SGTE solutions database and are based on the thermodynamic assessment contained within [12]. The phase diagram is shown in Figure 1.

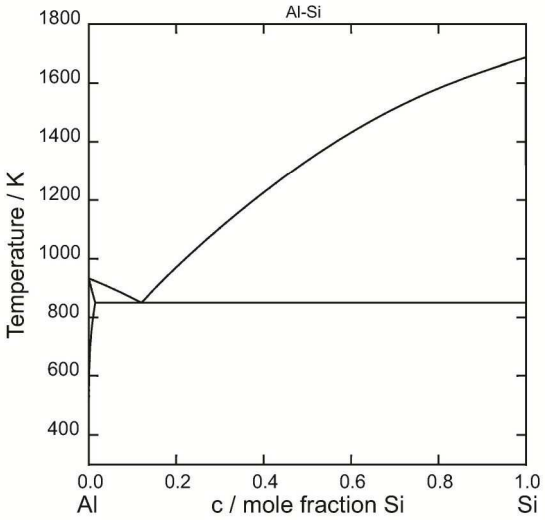

Figure 1. Phase diagram for the Al-Si system. Simulations here conducted at $c = 0.6$.

The solution to the above set of equations is obtained using a finite difference implicit scheme with a geometric multigrid solver on an adaptive mesh to achieve high a density of mesh elements at the interface. Full details of the computational scheme, applied to the growth of continuous (non-faceted) crystals, are given in [13].

Anisotropy and Modelling of Facets

The effect of the anisotropy function, γ, on the equilibrium shape of the crystal is shown in Figure 2. Figure 2a shows a polar plot of γ for several values of the anisotropy strength, ε. The corresponding Frank diagram is a contour of γ in $[\phi_x, \phi_y]$ space, where ϕ_x and ϕ_y are the partial derivative of ϕ with respect to x and y respectively. An example Frank diagram, corresponding to values of ε used in Figure 2a is shown in Figure 2b. From this we can calculate the function $W(t) = [\gamma_x(t), \gamma_y(t)]$, where $[\phi_x = \cos(t), \phi_y = \sin(t)]$ and:

$$\gamma_x \equiv \frac{\partial \gamma}{\partial \phi_x}, \quad \gamma_y \equiv \frac{\partial \gamma}{\partial \phi_y} \tag{10}$$

$W(t)$ is shown in Figure 2c and is in fact the well-known Wulff shape giving the equilibrium shape of the crystal. For high values of ε it can be seen from Figure 2c that $W(t)$ develops cusps or 'ears' aligned with the principal anisotropy directions. These correspond to disallowed crystal orientations and indicate that the resulting solidification morphology will develop a sharp vertex during growth. For n-fold symmetry this will occur for $\varepsilon > 1/(n^2 - 1)$, $\varepsilon > 1/15$ for four-fold growth. However, it is clear from Figure 2c that the Wulff shape still has curved sides even for $\varepsilon > 1/15$, that is high anisotropy strength *per se* does not yield a faceted crystal with flat faces.

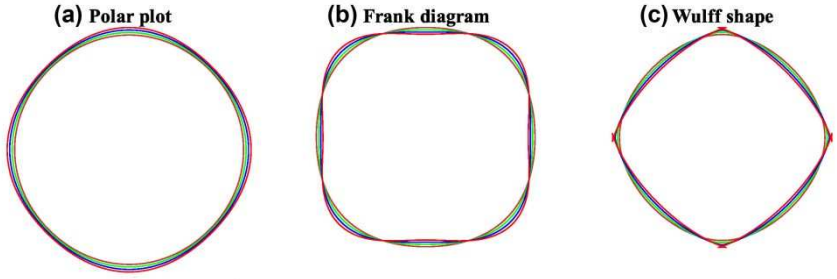

Figure 2. (a) Polar plot, (b) Frank diagram and (c) Wulff shape for a weak 4-fold anisotropy.

In fact, as shown in Figure 3, the condition for flat, i.e. faceted, faces is that polar plot of γ should have concave regions. For six-fold symmetry, as we might require for growth of Si crystals, this is achieved using an anisotropy of the form $(1 + |\varepsilon\cos(3\theta)|)$ and has been adopted within the phase-field code for the simulations reported here. However, the sharp vertices also associated with the Wulff shape for this anisotropy can cause numerical problems, wherein to avoid this we approximate $|\cos(3\theta)|$ by $\sqrt{(\cos 3\theta)^2 + q}$, where q is a small quantity. The effect is to introduce vertices which have a small, but constant curvature. Noting that:

$$\cos 3\theta = \cos^3\theta - 3\cos\theta\sin^2\theta = \frac{\phi_x^3 - 3\phi_x\phi_y^2}{|\nabla\phi|^3} \tag{11}$$

we have the final form of the anisotropy functional as:

$$\gamma = \left\{1 + \varepsilon \sqrt{\frac{\left(\phi_x^3 - 3\phi_x\phi_y^2\right)^2 + q^6}{\left(\phi_y^2 + \phi_y^2 + q^2\right)^3}}\right\} \nabla\phi \tag{12}$$

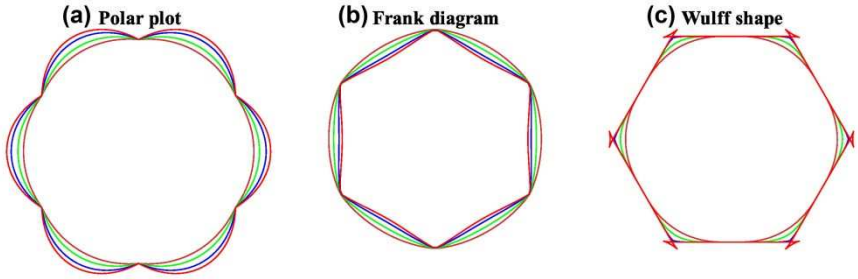

Figure 3. (a) Polar plot, (b) Frank diagram and (c) Wulff shape for a faceted hexagonal crystal.

Results and Discussion

Figure 4 illustrates the crystal morphologies simulated at four different nucleation temperatures; T_N = 1300 K, 1200 K, 1100 K and 1000 K. These are relative to a liquidus temperature at c = 0.6 of 1430 K. The progression from essentially flat faceted hexagonal crystal at the lowest undercooling to almost fully continuous six-fold dendrite at the highest undercooling is clear, showing that the proposed model provides an appropriate framework for simulating a faceted to continuous growth transition with increasing driving force. Further detail is given in Figure 5 in which we show the growth of the crystal at T_N = 1000 K at three different instances in time. A pseudo-3D contouring is used in Figure 5 as this is particularly effective in picking out the solute rich cores evident within the dendrite arms.

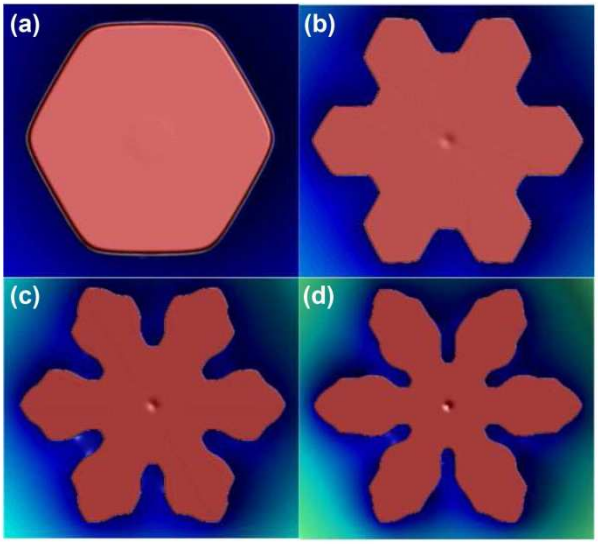

Figure 4. Crystal morphologies for nucleation temperatures of (a) 1300 K, (b) 1200 K, (c) 1100 K and (d) 1000 K. All have the same anisotropy function as shown in Figure 3.

In order to evaluate the evolution of the crystal morphology quantitatively as a function of time and undercooling we define Λ as:

$$\Lambda = \frac{Perimter^2}{4\pi \times Area} \tag{13}$$

This measure is invariant under scaling and is normalised so as to equal unity for a circle. Any other closed shape will have $\Lambda > 1$, with a regular hexagon having the value $\Lambda = 6/(\sqrt{3}\pi) \approx 1.10$. Figure 6 plots (a) Λ and (b) the rate of change of Λ, $\dot{\Lambda}$, both as a function of the maximum extent of growth. Larger values of Λ indicate increasing departure from the hexagonal morphology and hence a crystal with a more dendritic character.

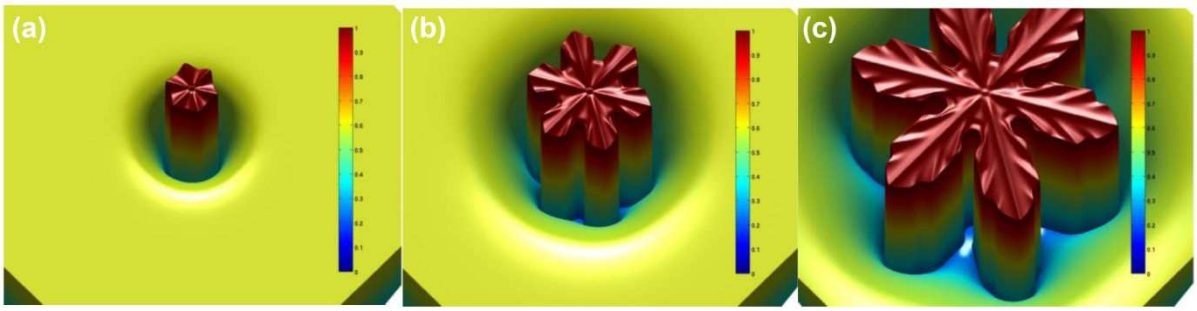

Figure 5. Three snapshots at different stages in the growth of a crystal with nucleation temperature of 1000 K.

With reference to Figure 6a it is clear that Λ increases as growth progresses at all undercoolings studied here. From Figure 6b it can be seen that in all cases $\dot{\Lambda}$ is initially positive but decreasing. This initial transient is as a result of the model using a circular seed to nucleate solidification. This is a deliberate choice so that any subsequent growth of an hexagonal morphology is unambiguously the result of the system selecting such a morphology, not being forced by the initial condition. In the case of the growth of a solid hexagon, Λ will increase from 1.00 to 1.10 and $\dot{\Lambda}$ will decrease monotonically tending asymptotically towards zero. This appears to be the behaviour observed at the highest nucleation temperature (lowest undercooling) of T_N = 1300 K. At nucleation temperatures of 1200 K and below, $\dot{\Lambda}$ passes through a local minimum, thereafter increasing rapidly. This corresponds to the point at which Λ initially exceeds 1.10 and as such is the first indication that the resulting crystal morphology will not be a simple regular hexagon. It can be seen from Figure 6b that all of the minima for different nucleation temperatures lie on a single straight line (in log-linear co-ordinates). Consequently, it would appear that the size of the crystal when it first begins to depart from simple hexagonal can be easily predicted for any given nucleation temperature. It is also clear that the curve for T_N = 1300 K has become asymptotic to the line and, as such, is unlikely to display a minimum. This would indicate tha for T_N = 1300 K a simple hexagonal crystal will be preserved indefinitely during growth, in line with expectation that close to equilibrium the Wulff shape is recovered.

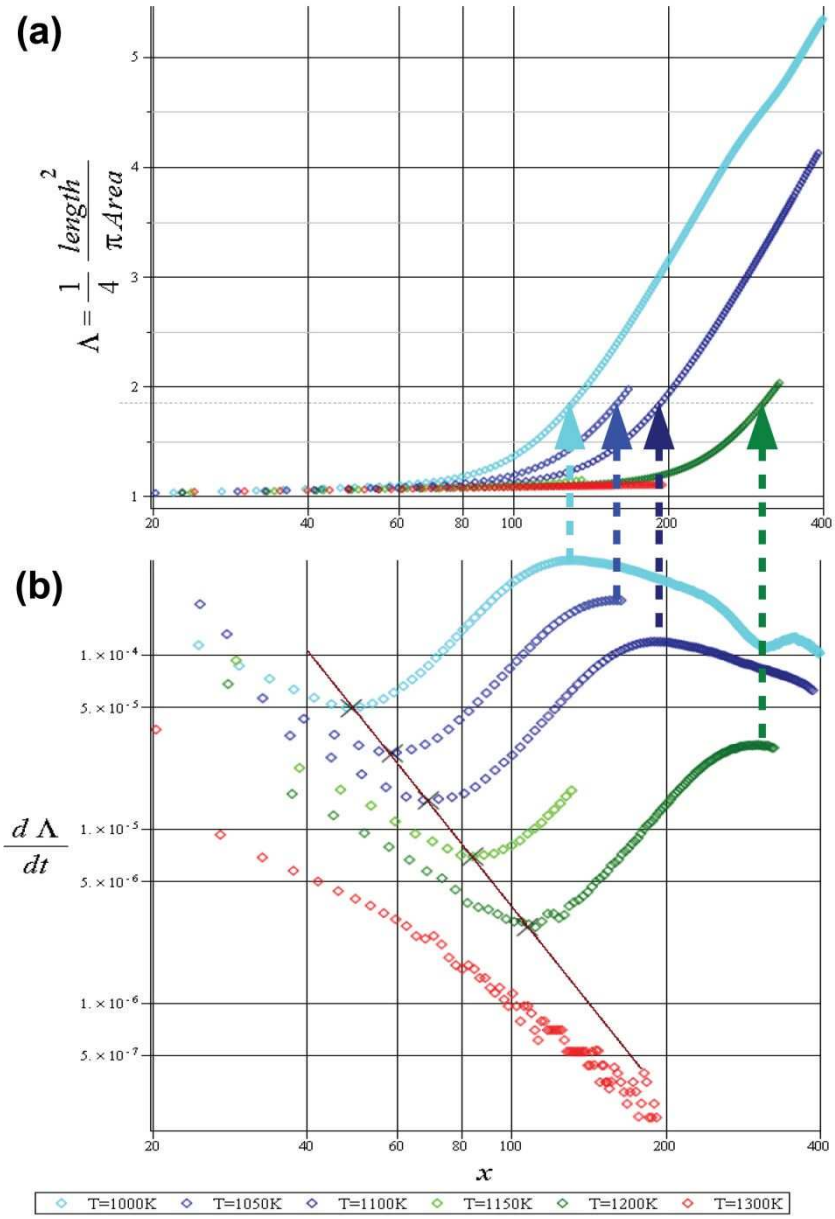

Figure 6. (a) Scaled ratio of (Perimeter)^2/Area as a function of crystal size for various nucleation tmperatures. (b) Rate of change of ratio of (Perimeter)^2/Area.

With continued growth, at all nucleation temperatures except T_N = 1300 K, $\dot{\Lambda}$ subsequently passes through a local maximum. Irrespective of undercooling, this occurs for $\Lambda \approx 1.75$ and corresponds to a morphology which we might loosely describe as a faceted hexagonal star, of which Figure 4b is an example. This rapid change in Λ (maximum in $\dot{\Lambda}$) seems to be related to the formation of arms along the original locations of the vertices. Thereafter, $\dot{\Lambda}$ mostly decreases smoothly, possibly with subsequent local minima, as evident in the curve for T_N = 1000 K. These probably correspond to the formation of the faceted kinks in the dendrite arms, as evident in Figure 5c.

Summary and Conclusions

A phase-field model for the binary alloy solidification of faceted crystal morphologies has been proposed. It has been demonstrated that not only can the model reproduce the Wulff shape for near equilibrium solidification, but that faceted to dendritic transitions can be simulated at large departures from equilibrium, in agreement with rapid solidification experiments. A scaled ratio of the (perimeter)^2 to the area of the crystal, denoted by Λ, is used as a measure of the departure of the morphology from the equilibrium Wulff shape. The evolution of Λ, and of its rate of change, $\dot{\Lambda}$, as a function of crystal size and undercooling, provides a framework in which the evolution of non-equilibrium crystal shapes may be understood.

References

[1] Taylor JE, Cahn JW (1998) Diffuse interfaces with sharp corners and facets: phase field models with strongly anisotropic surfaces, Physica D 112:381-411.

[2] Eggleston JJ, McFadden GB, Voorhees PW (2001) A phase-field model for highly anisotropic interfacial energy Physica D 150:91-103.

[3] Debierre J-M, Karma A, Celestini F, Guerin R (2003) Phase-field approach for faceted solidification, Physical Rev. E 68:041604.

[4] Uehara T, Sekerka RF (2003) Phase field simulations of faceted growth for strong anisotropy of kinetic coefficient, J. Cryst. Growth 254:251-261.

[5] Miura H (2013) Anisotropy function of kinetic coefficient for phase-field simulations: reproduction of kinetic Wulff shape with arbitrary face angles, J. Cryst. Growth 367:8-17.

[6] Lin HK, Chen HY, Lan CW (2014) Adaptive phase field modelling of morphology instability and facet formation during direction solidification of SiGe alloys, J. Cryst. Growth 385:44-48.

[7] Allen CM, O'Reilly KAQ, Cantor B, Evans PV (1998) Intermetallic phase selection in 1XXX Al alloys, Prog. Mater. Sci. 43:89-170.

[8] Panofen C, Herlach DM (2007) Solidification of highly undercooled Si and Si-Ge melts, Metal. Mat. Trans A, 449:699-703.

[9] Battersby SE, Cochrane RF, Mullis AM (1997) Highly undercooled germanium: Growth velocity measurements and microstructural analysis, Mater. Sci. Eng., A 226:443-447.

[10] Liu RB, Herlach DM, Vandyiousse M, Greer AL (2003) Morphologies of silicon crystals solidified on a chill plate, Metal. Mat. Trans A, 35A:1067-1073.

[11] Xian JW, Belyakov SA, Nogita K, Yasuda H, Gourlay CM (2017) Faceted and Nonfaceted growth of Cu_6Sn_5 crystals, in: Fan Z (ed.) *Proceedings of Solidification Processing 2017 (SP17)*, Brunel University UK, pp 251-254 (ISBN 978-1-908549-29-7).

[12] Groebner J, Lukas HL, Aldinger F (1996) Thermodynamic calculation of the ternary system Al-Si-C, CALPHAD 20:247-254.

[13] Bollada PC, Jimack PK, Mullis AM (2015) Three dimensional thermal-solute phase field simulation of binary alloy solidification, J. Comp. Phys. **287**:130-150.

Acknowledgements

This research was funded by the EPSRC Innovative Manufacturing Research Hub in Liquid Metal Engineering (LiME), Grant No. EP/N007638/1.